

FTD-ID(RS)T-0255-88

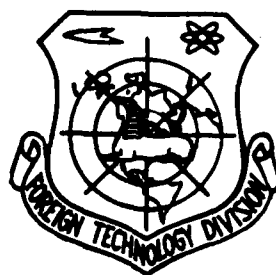
# FOREIGN TECHNOLOGY DIVISION



TRANSVERSE CO<sub>2</sub> LASER TWO-DIMENSIONAL GAIN DISTRIBUTIONS

by

Chen Liyin, Chu Zexiang, Chen Haitao



DTIC  
ELECTE  
JUL 19 1988  
S D  
C & E

Approved for public release;  
Distribution unlimited.

AD-A196 240

## HUMAN TRANSLATION

FTD-ID(RS)T-0265-88

24 June 1988

MICROFICHE NR: FTD-88-C-000513

TRANSVERSE CO<sub>2</sub> LASER TWO-DIMENSIONAL GAIN  
DISTRIBUTIONS<sup>2</sup>

By: Chen Liyin, Chu Zexiang, Chen Haitao

English pages: 17

Source: Jiguang, Vol. 11, Nr. 5, 1984,  
pp. 257-262

Country of origin: China

Translated by: SCITRAN

F33657-84-D-0165

Requester: FTD/TQTD

Approved for public release; Distribution unlimited.

THIS TRANSLATION IS A RENDITION OF THE ORIGINAL FOREIGN TEXT WITHOUT ANY ANALYTICAL OR EDITORIAL COMMENT. STATEMENTS OR THEORIES ADVOCATED OR IMPLIED ARE THOSE OF THE SOURCE AND DO NOT NECESSARILY REFLECT THE POSITION OR OPINION OF THE FOREIGN TECHNOLOGY DIVISION.

PREPARED BY:

TRANSLATION DIVISION  
FOREIGN TECHNOLOGY DIVISION  
WPAFB, OHIO.



# GRAPHICS DISCLAIMER

All figures, graphics, tables, equations, etc. merged into this translation were extracted from the best quality copy available.

Accession For	
NTIS GRA&I	<input checked="checked" type="checkbox"/>
DTIC TAB	<input type="checkbox"/>
Unannounced	<input type="checkbox"/>
Justification	
By _____	
Distribution/	
Availability Codes	
Dist	Avail and/or Special
A-1	

↓

SUMMARY: Using one-dimensional gas flows and quasi-two-dimensional electrical discharge models, we calculated the two-dimensional gain curve contour lines for equal values on perpendicular electrode planes. We studied the electrical discharge area gas flow speeds and electrical discharge parameters as well as gas constituents and similar items and their effects on the rules or patterns of changes along the direction of the gas flow. As far as each gas pressure is concerned, they had flow speed ranges which corresponded to optimum gain curves. We took calculation results and experimental results and carried out a comparison. *Demaria, translation, 1972*

This article studies, in electrical discharge areas, the electrical discharge transverse flow  $\text{CO}_2$  laser, with its three mutually perpendicular directions or axes for light axis, electrical current direction, and gas flow direction. In these electrical discharge areas, at the same time, one sees the occurrence of molecular (atomic) ionization and compounding, electron state and vibrational state electrical excitation, collision relaxation fading of laser stimulation in the various sets of dimensions, as well as, light absorption, radiation, oscillation and other similar processes. These formed a type of complex, non-equilibrium flow movement problem. Past theoretical work led to the understanding and analysis of a great deal. However, due to the fact that the models were overly simplified, it was difficult to make detailed descriptions of gain peculiarities. For example, T.A. Cool [1] and H.A. Hassan [2] did work in which it was assumed that the electrical excitation occurs in the upper reaches of the light cavity, before the gas flow enters the light cavity and that there already is particle number inversion. In the light cavity, there are only molecular collision processes and light absorption, excitation, and radiation processes. A.J. Demaria [3] and others only solved, under stable state conditions, for the speeds of processes, and have not yet been able to obtain the distribution of gain coefficients in total excitation areas. E. Armandillo [4], on the subject of parallel plate electrode transverse flow laser theory and experimentation, did an exhaustive analysis. However, in order to overcome the difficulties of calculations, he selected for use a type of current flow distribution which was capable of making the calculations and the results of experiments agree with each other. Moreover, he assumed that the  $\text{CO}_2$  ionization reached

50%. This type of method has a relatively large localization. All the above work is set up on the basis of a one-dimensional analysis. But, experimentation still indicates that the gain coefficient number has a two-dimensional distribution [5,6]. This article presents a type of simplified one-dimensional gas flow and quasi-two-dimensional electrical discharge model, using numerical value calculation methods to quantify or semi-quantify simulated two-dimensional gain distributions along flow movement directions perpendicular to electrode planes as well as the effects of flow movement parameters on gain distributions.

258

## I. THEORETICAL MODELS

Electrical discharge models: consider an electrode structure of a form in which a metallic plate ABCD is the anode, EE'K'K is the cathode (it is possible that these could be tubes or plates or needles), and the perpendicular distance between the electrodes  $AE=H$  (Fig. 1). The working gases enter from the plane AEKD. Between the two electrodes, one adds an appropriate voltage, producing fluorescent electrical discharge, forming an electrical discharge area the side area of which is AEFB with a length of  $L$ . Except for the dark area in the vicinity of the cathode EE'K'K, and the dark area in the vicinity of the anode ABCD, the other large segments are regular column areas. If we assume that the gas temperature, the flow speed, the pressure, and the current density, as well as other similar macro quantities along the direction of the  $y$  axis are all the same, but, that in the two directions of the  $x$  and  $z$  axes there are still differences, we form a two-dimensional graph for the  $x$ - $z$  plane. If we again assume that, in the gas flow, the momentum, mass, and energy transmission process along the  $z$  direction can be disregarded, approximately taking each  $x$ - $y$  planar layer and seeing it as standing on its own, it is only necessary to give, at a certain altitude, the current density and the electrical field strength, and, it is then possible, for that height or altitude, to carry out one-dimensional gas dynamics calculations, obtaining one-dimensional distributions for the  $x$ - $y$  plane in question, showing the gas flow temperature, concentration, and small signal gain. Again, we carry out calcu-

(i) 图1 放电柱区

Within normal column areas, the current density  $j$  is distributed according to equation (1), and, it is a function of the height  $z$ :

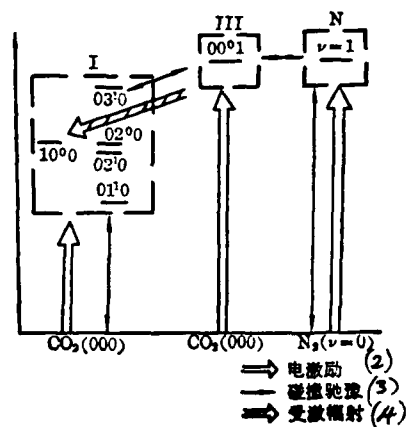
In this equation, J is the overall current.  $a=AB$ .  $b=EF$ . H is the distance between electrodes. By adjusting a, b, H, and L, it is possible to flexibly change the current density on the x-z plane, using the appropriate machine configuration and placement.

$$n_i = \frac{j}{v_{De}} \quad (2)$$

In the equation,  $v_D$  is the electron transition speed.  $e$  is the electron electric charge.

On the cathode surface and in the vicinity of the dark space, electron movement speeds are very small. Effective vibrational emission speeds are also very small. Because of this, the effective electron density is zero. In order to satisfy this one condition, we assume that, beginning from a certain place in the vicinity of the cathode, the electron density, according to the sine function numbers, gradates toward zero in the direction of the cathode.

As far as parallel electrode plates are concerned, the electric field  $E$  is a constant. However, because of the fact that, along the  $x$  direction, the gas flow temperature gradually goes up, the particle number density  $n$  correspondingly decreases. Therefore, this  $E/n$ , along the  $x$  direction, gradually goes up. As far as needles (tubes) go, as compared to plate electrodes,  $E$ , along the  $x$  direction, goes down.  $n$  is also reduced along the  $x$  direction. Experiments demonstrate [5] that  $E/n$ , in regular columnar areas, does not experience large changes. In these areas, one can approximate it with constants.



(1) 图2 能级图

1. Fig.2 Energy Level Chart 2. Electrical Excitation 3. Collision Relaxation 4. Stimulated Amplitude of Radiation

In regular columnar areas, the interval between gas molecules as well as the interval between molecules and electrons shows the existence of frequent collisions. Moreover, carrying out energy transfer, their process can be described simply by the use of Fig. 2. We assume that rotation and flat motion take place at equilibrium. Moreover, we ignore ionization and the disintegration reaction of  $\text{CO}_2$  under the effects of electrons. According to traditional methods, one takes  $\text{CO}_2$  and  $\text{N}_2$  molecules and simplifies their vibrational states to be the mutually independent simple vibration forms I, III and N. Each vibrational form is a resonance particle, and, using the vibration temperature  $T_i$  in order to describe it, the particle number uses the Boltzmann distribution expression:

259

$$n_i^{(l)} = n_i^{(0)} e^{-\frac{lh\nu_i}{kT_i}} \quad (3)$$

$n_i^{(l)}$  expresses the  $i$  vibration form  $l$ th vibration energy level particle number density.  $\nu_i$  is the frequency.  $T_i$  is the vibrational temperature.  $h$  and  $k$  respectively are Planck's and Boltzmann's constants.

On the basis of Fig. 2, the particle number formation rates for the three vibration forms appear in the equations:

$$\frac{dn_1}{dt} = \left( \frac{dn_1}{dt} \right)_{\text{辐射}}^{(1)} + \left( \frac{dn_2}{dt} \right)_{\nu_1 \rightarrow 2} \quad (4)$$

$$+ \left( \frac{dn_3}{dt} \right)_{\nu_1 \rightarrow 3\nu_1} + \left( \frac{dn_3}{dt} \right)_{\text{电激励}}^{(2)}$$

$$\frac{dn_3}{dt} = \left( \frac{dn_3}{dt} \right)_{\nu_1 \rightarrow 3\nu_1} + \left( \frac{dn_3}{dt} \right)_{\nu_1 \rightarrow \nu_3} \quad (5)$$

$$+ \left( \frac{dn_3}{dt} \right)_{\text{辐射}}^{(3)} + \left( \frac{dn_3}{dt} \right)_{\text{电激励}}^{(4)}$$

$$\frac{dn_N}{dt} = \left( \frac{dn_N}{dt} \right)_{\nu_N \rightarrow \nu_1} + \left( \frac{dn_N}{dt} \right)_{\nu_N \rightarrow 2} \quad (6)$$

$$+ \left( \frac{dn_N}{dt} \right)_{\text{电激励}}^{(5)}$$

1. radiation 2. electrical excitation 3. radiation 4. electrical excitation 5. electrical excitation

Each  $\left(\frac{dn_i}{dt}\right)$  quantity can be seen in reference [7] at appendix B.

## II. MATHEMATICAL EXPRESSIONS

In regular columnar areas, at each altitude or height, the gas flow is a steady state one-dimensional ideal gas, obeying the conservation equation set below:

$$\frac{d}{dx}(\rho u) = 0 \quad (7)$$

$$\rho u \frac{du}{dx} + \frac{dp}{dx} = 0 \quad (8)$$

$$\frac{d}{dx}\left(h + \frac{u^2}{2}\right) = \frac{jE}{\rho u} - \frac{1}{\rho u} \frac{dq}{dx} \quad (9)$$

$$u \frac{dn_i}{dx} = \omega_i \quad (i=2, 3, N) \quad (10)$$

$$p = \rho \frac{R}{M} T \quad (11)$$

In these equations,  $\rho$ ,  $u$ ,  $p$ ,  $h$ ,  $E$ ,  $\omega_i$  and  $M$  respectively represent gas density, flow speed, pressure, the enthalpy of each gram of gas, electrical field strength, dynamic speed and the molecular weight of compounds. Because, here, consideration is not given to heat transfer, and there is also no laser output, it follows that

$$\frac{dq}{dx} = 0.$$

The right end of equation (10) is expressed by equation set (4)-(6). Take equation (9) and integrate it against  $x$ . After rearranging, one gets

$$T = \frac{h_0 - HV - EU + EX}{\frac{R}{M} \left[ \frac{7}{2} (\psi_{CO_2} + \psi_{N_2}) + \frac{5}{2} \psi_{He} \right]} \quad (12)$$

In this, HV is the vibration energy,

$$EX = \frac{jE}{\rho_0 u_0} x, \quad EU = \frac{1}{2} (u_0^2 - u^2),$$

The subscripts express the regular columnar entry conditions.  $\psi_M$  is the component M in the molecular percentage of the gas compound. M = 1,2,3 represents CO<sub>2</sub>, N<sub>2</sub>, and He. From equations (7), (8), and (11), it is possible to derive:

$$u = \frac{1}{2} \left( B \pm \sqrt{B^2 - 4(R/M)T} \right) \quad (13)$$

$$P = P_0 + \rho_0 u_0^2 - \frac{1}{2} \rho_0 u_0 \left( B \pm \sqrt{B^2 - 4(R/M)T} \right) \quad (14)$$

In this,  $B = (P_0 + \rho_0 u_0^2) / \rho_0 u_0$ .

The computational procedure is: given the entry parameters  $T_0$ ,  $P_0$ ,  $u_0$ ,  $\psi_M$  and the regular columnar formation a, b, H, L, and j, as well as E distribution, take the equation set (4)-(6) and (12) and couple them to derive  $n_i$  and T. Integrate beginning from x=0 straight through until after the end of BCGF. From equation (3), derive  $T_i$ . From equations (11), (13), and (14), derive  $P$ ,  $u$ ,  $\rho_0$ . Take the derived  $n_{100}$  and  $n_{001}$  and substitute them into equation (15). It is then possible to derive the small signal gain  $G_0$  along the x axis for a certain altitude value z.

$$G_0 = \left( \frac{\lambda^2}{4\pi \tau_{21} \nu_0} \right) \times \left( n_{001} \frac{43.4}{T} e^{-\frac{211.5}{T}} - n_{100} \frac{46.0}{T} e^{-\frac{235.6}{T}} \right) \quad (15)$$

In the equation,  $\lambda = 10.6$  microns.  $\tau_{21}$  is the spontaneous radiation life (5.38 sec).  $\nu_0$  is the collision frequency. Due to the fact that operational pressure is relatively high, here, consideration is only given to pressure widening.

Using the Rugge-Kutta (phonetic approximation) method, we carried out a numerical value integration. The electrical excitation speed parameter which is used, the electron transition speed, and the electron temperature are all selected from [8]. The collision relaxation speed parameter which is used is selected from [9-12].

### III. CALCULATION RESULTS AND DISCUSSION

The primary parameter ranges which this article calculates are:  $T_0 = 293K$ .  $P_0 = 20-50$  (ton).  $u_0 = 30-310$  m/sec. The gas constituents are  $[CO_2] : [N] = [0.03-0.05] : [0.29-0.71]$ . The rest is [He].

260

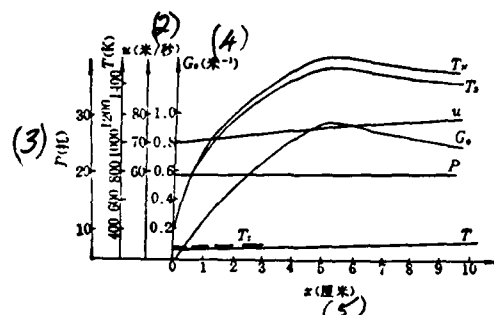
$j = 10-30$  mAmp/sq.cm,

$E/n = (1.9-3.0) \times 10^{-16}$  volts.sq.cm.

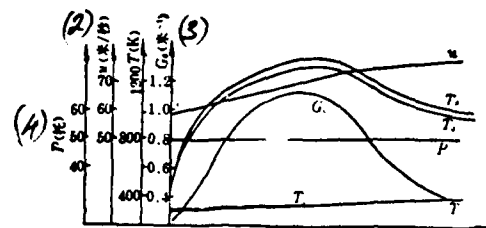
Figs. 3-7 are the calculated values for the small signal gain and flow movement parameters along the direction of the flow movement at locations where the height or altitude is  $z=1.5$ cm. From these Figs. it is possible to see that the gas flow pressure  $P$  along the  $x$  direction does not change greatly. The temperature  $T$  and the speed  $u$  show a general rise.  $T$  is approximately equal to  $T_2$ . And  $T_x$  is generally larger than  $T_2$ . If one continues to raise the gas flow speed, then, the calculated values for maximum temperature rise and

maximum speed difference go down. This is shown in Table 1. This explains why the flow speed increase is capable of effectively eliminating waste energy. It is capable of overcoming the lower energy level blockage caused by the temperature increase and creating a bottleneck effect for the gain drop. This is the advantage of the flow movement laser device over the static laser. Because of this, the gas flow pressure  $P$  is capable of going up a certain amount.

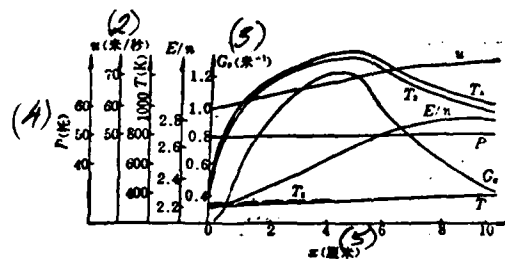
The primary difference between the areas in Fig. 3 and Fig. 4 is that the gas flow pressures are not the same. In Fig. 4, the various parameter curves along the  $x$  direction all show changes which are comparatively steeper than those in Fig. 3. This explains the reason why increases in the pressure have relatively large effects on the laser emission dissipation reaction of collisions between molecules. Fig. 6 shows that, when the relative or specific electric power is not greatly changed, the pressure increase will cause the small signal gain  $G_0$  along the  $x$  direction to go down relatively fast.



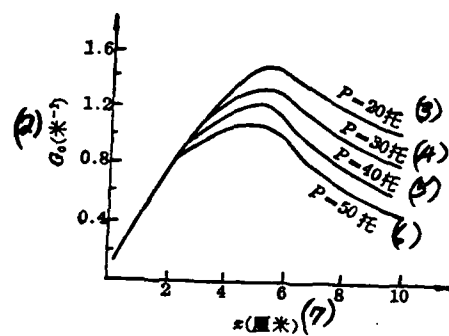
1. Fig. 3 Changes in  $T, T_i, u, P, G_0$  Along the  $x$  Direction  $E/n=2.2 \times 10^{18}$  volt.sq.cm;  $\psi_1:\psi_2:\psi_3 = 0.05:0.27:0.68$ ;  $MN=5$ cm;  $P_0 = 20$  ton
2. m/sec 3. ton 4. m 5. cm



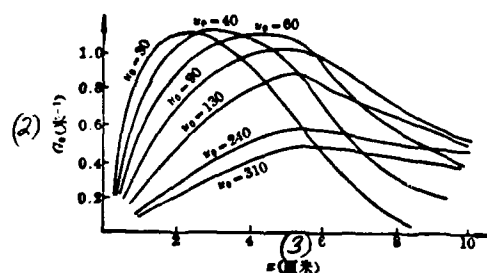
1. Fig. 4 Changes in  $T, T_i, u, P, G_0$  Along the  $x$  Direction.  
 $E/n = 2.2 \times 10^{-16}$  volt.sq.cm.;  $\psi_1 : \psi_2 : \psi_3 = 1 : 2 : 7$ ;  $MN = 5$  cm;  $P_0 = 50$   
 ton 2. m/sec 3. m 4. ton



1. Fig. 5 Changes of  $T, T_i, u, P, G_0, E/n$  Along the  $x$  Axis.  $P_0 = 50$  ton;  
 $(E/n)_0 = 2.2 \times 10^{-16}$  volt.sq.cm.;  $\psi_1 : \psi_2 : \psi_3 = 1 : 2 : 7$ ;  $MN = 5$  cm  
 2. m/sec 3. m 4. ton 5. cm



1. Fig. 6  $G_0 - P_0 \sim x$  Graph  $E/n = 2.2 \times 10^{-16}$  volt.sq.cm.;  $u_0 = 30 \text{ m/sec}$ ;  $T_0 = 293 \text{ K}$ ;  $\psi_1 : \psi_2 : \psi_3 = 1 : 2 : 7$ ;  $MN = 5 \text{ cm}$  2. m 3. ton 4. ton 5. ton 6. ton 7. cm



1. Fig. 7  $G_0 - u_0 \sim x$  Graph  $E/n = 2.2 \times 10^{-16}$  volts.sq.cm.;  $P_0 = 50 \text{ ton}$ ;  $T_0 = 293 \text{ K}$ ;  $\psi_1 : \psi_2 : \psi_3 = 1 : 2 : 7$ ;  $MN = 5 \text{ cm}$  2. m 3. cm

(1) 表1 流速和温升、速度增量关系

P (托)	50							20
CO <sub>2</sub> :N <sub>2</sub> :H <sub>2</sub>	1:2:7							5:25:70
u <sub>0</sub> (米/秒)	30	40	60	90	130	240	310	70
u-u <sub>0</sub> (米/秒)	18	17	16	15	14.5	14	16	19
T-T <sub>0</sub> (°C)	175	130	80	47	30	11	7	37

$x=10$  厘米,  $T_0=293$  K,  $MN=5$  厘米,  $E/n=2.2 \times 10^{-16}$  伏·厘米

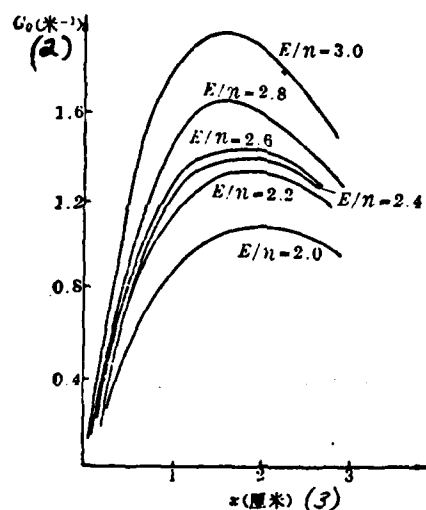
1. Table 1 The Relationships Between Flow Speed, Rises in Temperature, and Increases in Speed 2. ton 3. m/sec 4. m/sec 5. cm 6. cm 7. volt.sq.cm.

261

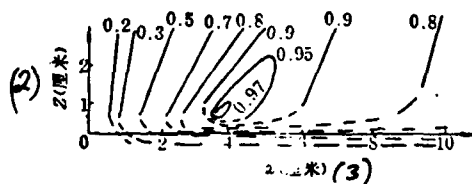
The difference between Fig. 4 and Fig. 5 lies in the fact that the changes in  $E/n$  along the  $x$  direction are not the same. In Fig. 4,  $E/n$  is a constant. In Fig. 5,  $E/n$  along the  $x$  axis goes up ( $E$  is approximately equal to a constant.  $n$  along the  $x$  axis goes down. This is with the use of simulated parallel plate electrodes.) In Fig. 4, the peak gain value is  $1.0 \text{ m}^{-1}$ . In Fig. 5, the peak gain value is  $1.3 \text{ m}^{-1}$ . Also,  $u$  and  $T$  go up quickly.

When the externally added electric power does not change, from Fig. 7, we can see that  $u_0$  rises from 30 m/sec to 70 m/sec. The peak gain value is basically unchanged. It is just that the location of the peak value is shifted back. The effective gain surface area is expanded. Because of this, we arrive at the conclusion that, for a certain operating pressure, there exists an optimum flow speed range. If one excessively increases the flow speed, there is no attendant advantage. In Fig. 7,  $P_0 = 50$  tons. The  $G_0 \sim u_0 \sim x$  relationship for  $u_0 = 60-70$  m/sec is basically in line with the experimental results in [6]. The difference lies in the fact that the experimental value for  $G_0$  along  $x$  goes down relatively fast. This is due to the fact that, in our calculations, we selected for use a uniform distribution along the  $x$  direction for current density.

Fig. 8 gives, for the same operating conditions, the  $G_0 \sim x$  graph when there are different  $E/n$ .  $G_0$  increases with  $E/n$ , and rapidly rises. However, after it reaches a peak value, it goes down at even a somewhat steeper rate. The amount of mass flow does not change. The rise in the value of  $E/n$  signifies an increase in specific or comparative power. At the current experimental levels, an increase in the specific electric power can easily produce electrical arcing, destroying normal operation. If it is possible to overcome this difficulty, an appropriate increase in the value of  $E/n$  is advantageous for an increase in gain.

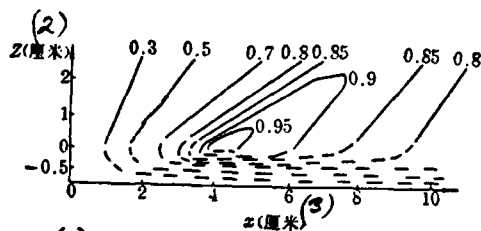


1. Fig. 8  $G_0 \sim E/n \sim x$  Relationship Graph  $u_0 = 70 \text{ m/sec}$ ;  $P_0 = 50 \text{ tons}$ ;  $T_0 = 293\text{K}$ ;  $\psi_1:\psi_2:\psi_3 = 1:2:7$ ;  $MN = 3\text{cm}$ ;  $E/n = (2.0-3.0) \times 10^{-16} \text{ volt.sq.cm.}$  2. m 3. cm



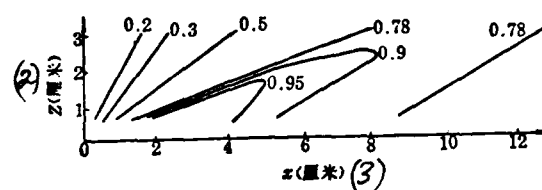
(1) (a) 梯形辉光区中的等增益分布图  
 $AB=5.5$  厘米;  $EF=2.9$  厘米;  $H=3$  厘米

1. (a) Equal Gain Distribution Graph in Gradient Flourescence Areas  $AB=5.5\text{cm}$ ;  $EF=2.9\text{cm}$ ;  $H=3\text{cm}$  2. cm 3. cm



(1) (b) 梯形辉光区中的等增益分布图  
 $AB=8$  厘米;  $EF=3$  厘米;  $H=3$  厘米

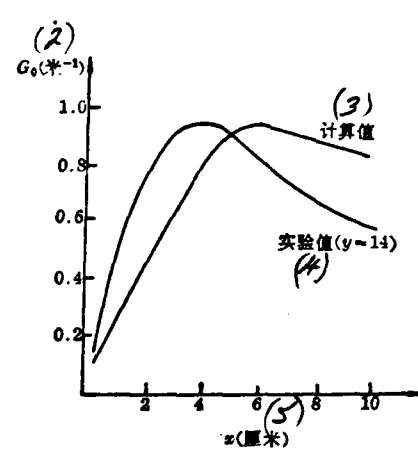
1. (b) Equal Gain Distribution Graph in Gradient Form Flourescence Areas  $AB=8\text{cm}$ ;  $EF=3\text{cm}$ ;  $H=3\text{cm}$  2. cm 3. cm Areas



(1) (c) 三角形辉光区中的等增益分布图  
 $\Delta B=10$  厘米;  $H=3$  厘米

(c) Equal Gain Distribution Graph in Triangular Form  
 Fluorescence Areas  $AB=10\text{cm}$ ;  $H=3\text{cm}$

Fig. 9 Equal Gain Curve Graphs



1. Fig.10 Comparison of Calculations and Experiments  $u_0 = 70 \text{ m/sec}$ ;  $P_0 = 20 \text{ tons}$ ;  $T_0 = 293\text{K}$ ;  $E/n = 2.2 \times 10^{-16} \text{ volts.sq.cm.}$ ;  $\psi_1:\psi_2:\psi_3 = 5:27:68$ ,  $MN=5.5\text{cm}$  2. m 3. Calculated Value 4. Experimental Value 5. cm

Fig. 9 shows the equal gain curve graphs for the x-z plane. (a), (b), and (c) represent the calculated results for three types of different regular columnar area forms. These graphs are similar to the experimental curves in [5,6]. However, the curve dispersal intervals are different. The reason for this is that, in reference [6], the lower part of the cathode has a section of cold gas flow through it, mixing with the laser activation medium and reducing the electron density. Because of this, the lower area experimental curves are drawn together and are not terribly similar to this model. In reference [5], because the pressure is very high, the curves are naturally compressed together.

Fig. 10 gives a comparison of the  $y=14$  curves calculated in this article and Fig. 4 in [6]. The theoretical and empirical curves for peak gain values do not differ much. However, the positions for the former peak values are moved considerably back. Moreover, the gain changes behind the peak value are relatively even and slow. The main problem is that this article assumes, in regular columnar areas, that the current density along the x direction is uniform. In reality, due to electron diffusion and incoming flow shock, the fluorescence area is moved back, and  $n_x$  along the x direction is certainly not uniform.

#### IV. CONCLUSION

Due to the fact that we selected for use a uniform current distribution model, all the physical quantities created show relatively even values in their changes along the x direction. If it is possible to select for use even more appropriate current distributions and field strength distributions, this will cause the calculation results to be even better.

From calculation results, one can see that it is only necessary that, for the various z layers, the entry parameters be the same. Because the flow movement parameters given rise to by the introduction of current show very small changes along the z direction, taking the calculation results at the position  $x=4\text{cm}$  as an example, when z changes from 0 to  $H=3\text{cm}$ , and,  $\Delta u \sim 3$  m/sec.  $\Delta T \sim 8\text{K}$  K., and  $\Delta P \sim 0$ .

This explains why ignoring the momentum, mass, and energy transfer for different z planes is feasible.

My thanks go to my comrades on the  $\text{CO}_2$  flow movement laser experiment team for their helpful discussion and assistance.

#### REFERENCES

- [1] T. A. Cool; *J. Appl. Phys.*, 1969, **40**, No. 9, 3563.
- [2] H. A. Hassan *et al.*; *AIAA J.*, 1972, **10**, 414.
- [3] A. J. Demaria *et al.*; *AIAA Paper*, No. 71-63.
- [4] E. Armandillo, A. S. Kaye; *J. Phys. D. Appl. Phys.*, 1980, **13**, No. 2, 321~328.
- [5] Toshimitsu Akiba *et al.*; *IEEE J. Quant. Electr.*, 1979, **QE-15**, No. 3, 162.
- [6] 赵建荣等;《中国激光》, 1983, **10**, No. 10, 743.
- [7] R. K. Seals; *AIAA Paper*, No. 71-588.
- [8] G. Befef ed. "Principles of Laser Plasmas", John Wiley and Sons, Inc., 1976, p. 394.
- [9] R. L. Taylor *et al.*; *Review of Modern Physics*, 1969, No. 4, 1.
- [10] Gen Inoue; *J. Phys. Soc. of Japan*, 1975, **38**, No. 3, 870.
- [11] J. T. Yarell; *JCP*, 1967, **46**, No. 11, 4491.
- [12] C. B. Moore; *JCP*, 1967, **46**, 4222.
- [13] J. C. Stephenson; *JCP*, 1971, **54**, No. 7, 3097.

[6] Zhao Jianrong, et.al.; "Chinese Lasers", 1983, **10**, No.10, 743.

# DISTRIBUTION LIST

## DISTRIBUTION DIRECT TO RECIPIENT

<u>ORGANIZATION</u>	<u>MICROFICHE</u>
A205 DMAHTC	1
A210 DMAAC	1
C509 BALLISTIC RES LAB	1
C510 R&T LABS/AVEADCOM	1
C513 ARRADCOM	1
C535 AVRADCOM/TSARCOM	1
C539 TRASANA	1
C591 FSTC	4
C619 MIA REDSTONE	1
D008 MISC	1
E053 HQ USAF/INET	1
E404 AEDC/DOF	1
E408 AFWL	1
E410 AD/IND	1
E429 SD/IND	1
P005 DOE/ISA/DDI	1
P050 CIA/OCR/ADD/SD	2
AFTT/LDE	1
FTD	
CCV	1
MIA/PHS	1
LLYL/CODE L-389	1
NASA/NST-44	1
NSA/T513/TDL	2
ASD/FTD/TQLA	1
FSL/NIX-3	1